Applied Surface Science 255 (2009) 4425–4429

Contents lists available at ScienceDirect

Applied Surface Science

journal homepage: www.elsevier.com/locate/apsusc

Structure and mechanical properties of reactive sputtering CrSiN films

Guangan Zhang [a,b,*], Liping Wang [a], S.C. Wang [c], Pengxun Yan [b], Qunji Xue [a]

[a] State Key Laboratory of Solid Lubrication, Lanzhou Institute of Chemical Physics, Chinese Academy of Sciences, Lanzhou 730000, PR China
[b] School of Physics Science & Technology, Lanzhou University, Lanzhou 73000, PR China
[c] National Centre for Advanced Tribology at Southampton (nCATS), School of Engineering Sciences, University of Southampton, SO17 1BJ, UK

ARTICLE INFO

Article history:
Received 27 May 2008
Received in revised form 16 November 2008
Accepted 17 November 2008
Available online 21 November 2008

PACS:
62.20.−x
62.20.Qp
68.35.Gy
81.40.Pq
87.15.La

Keywords:
CrSiN films
Magnetron sputtering
Microstructure
Mechanical properties

ABSTRACT

CrSiN films with various Si contents were deposited by reactive magnetron sputtering using the co-deposition of Cr and Si targets in the presence of the reactive gas mixture. Comparative studies on microstructure and mechanical properties between CrN and CrSiN films with various Si contents were carried out. The structure of the CrSiN films was found to change from crystalline to amorphous structure as the Si contents increase. Amorphous phase of Si_3N_4 compound was suggested to exist in the CrSiN film. The growth of films has been observed from continuous columnar structure, granular structure to glassy-like appearance morphology with the increase of silicon content. The film fracture changed from continuous columnar structure, granular structure to glassy-like appearance morphology with the increase of silicon content. Two hardness peaks of the films as function of Si contents have been discussed.

1. Introduction

Although transitional metal nitride films, such as CrN and TiN, have attracted a lot of interests due to the high hardness, high melting point and high chemical stability [1–3], their potential properties have not been fully achieved and the applications are limited. To explore these potential mechanical and especially high-temperature properties, many efforts have focused on the development of complex hard film materials. Recently, it was found that the deposits of multilayer or nanocomposite films improved the mechanical properties [4–8]. Veprek [6] first reported the TiSiN films with hardness exceeding 70 GPa by chemical vapor deposition (CVD). The addition of Si to TiN films has been shown to refine the grains through the formation of a nanocomposite structure of nanocrystalline (nc) TiN grains in an amorphous (a) matrix of Si_3N_4 (nc-TiN/a-Si_3N_4) [6,8–10]. Subsequent investigations were followed on nc-MeN/a-Si_3N_4 (Me = Cr, Zr, Nb, Mo) nanocomposites [11,7,12–14]. This composite structure of thin amorphous matrix and the crystallites was suggested to hinder the crack formation and propagation. However, there is still a dispute on the effects of Si addition to MeN on the bonding structure, crystalline structure and texture of the nanocomposite MeSiN films. The previous investigations on CrSiN films lack systematic research on the microstructural and mechanical properties by addition of Si [11,7,15–19]. The knowledge and characterization of these parameters are import to understand both the process involved in the preparation and the future behavior of such films.

In this paper, CrSiN films were synthesized using medium frequency reactive magnetron sputtering. The main objective was to investigate the effect of incorporated Si on the structure modification and mechanical properties of CrN films.

2. Experimental process

The CrN films with various Si contents were deposited on silicon p (1 1 1) wafer using medium frequency magnetron sputtering. The frequency of the power supply was fixed at 20 kHz at all the deposition process. The experimental equipment has been described in Ref. [20], so only is a brief description of experiment

* Corresponding author at: State Key Laboratory of Solid Lubrication, Lanzhou Institute of Chemical Physics, Chinese Academy of Sciences, Lanzhou 730000, PR China. Tel.: +86 931 4968335; fax: +86 931 4968335.
E-mail address: gazhang@lzb.ac.cn (G. Zhang).

0169-4332/$ – see front matter © 2008 Published by Elsevier B.V.
doi:10.1016/j.apsusc.2008.11.036

given here. A pair of magnetron planar Cr (99.8 wt.% in purity) and Si (99.8 wt.% in purity) targets with size of 280 mm × 80 mm × 8 mm were set in cylindrical vacuum chamber wall. The sputtering chamber was evacuated to a pressure of 4.0×10^{-3} Pa by a turbomolecular pump and then sputtering gas was introduced. The Si and mirror polished copper substrates were cleaned ultrasonically in acetone followed by de-ionized water. Then the Si substrates were glowing cleaned for 10 min at 1 Pa argon pressure at the substrate bias of −700 V. The film deposition process was carried out for 2 h at a 40 sccm Ar flow rate and a 160 sccm N_2 flow rate with the substrate bias at −100 V power at 1.1 kW (465–470 V × 2.4 A). To obtain the different Si/(Cr + Si) ratio of the CrSiN films, the specimens were placed at varying intervals between the Cr and Si targets. CrN films without Si were also deposited for the reference.

Film crystallinity and phase structure were characterized using grazing incidence X-ray diffraction (GIXRD). A Philips X'perts X-ray diffractometer with Cu Kα radiation was employed to test the thin films. The scanning was performed from 20° to 90° at an incident angle 1°. The Si/(Cr + Si) ratio of the CrSiN films deposited on the copper wafer surface were determined by energy dispersive X-ray spectroscopy (EDS) analysis in a JSM-5600 Lv scanning electron microscopy (SEM). X-ray photoelectron spectroscopy (XPS) analysis has been carried out on PerkinElmer PHI-5702 multi-functional photoelectron spectrometer with Al Kα radiation (1476.6 eV). The XPS spectra were collected in a constant analyzer energy mode, at a chamber pressure of 10^{-8} Pa and pass energy of 29.4 eV, with 0.125 eV/step. Fourier transformation infrared spectra of the films were recorded on a Bruker IFS66V Fourier transformation infrared spectrometer. By using transmission mode, the spectrum was collected for 500 scans at a resolution of 4 cm^{-1}. Field emission-SEM (Hitachi, S-4800) was utilized to observe the cross-sectional microstructure. The hardness of the films was determined by a nano-indenter (MTS Systems Corporation) using a Berkovich diamond tip and continuous stiffness option, with the maximum indentation depth within 100 nm (less than 10% of total film thickness to minimize the substrate contribution). Five replicate indentations were made for each film sample and the hardness was calculated from the load-unloading curves. Oliver and Pharr analysis method [21] was employed to calculate hardness values.

3. Results and discussions

3.1. Synthesis and characterization of CrSiN films

The CrSiN films with 6 different Si/(Cr + Si) ratios from 8.4% to 47.0% have been successfully deposited, in addition to the reference CrN film. The relative compositions of the CrSiN films determined by EDS are shown in Table 1.

Fig. 1 shows the XRD patterns of CrSiN films deposited on silicon wafer with various Si contents as well as the XRD pattern of CrN film for comparison. The XRD peaks in the CrN film are consistent to the diffraction peaks of cubic NaCl-type structure. For the CrSiN films up to 36.8 at.% Si, the XRD peaks are similar to that

Table 1
The composition and (1 1 1) peak position of the CrSiN films.

Si content (at.%)	Cr content (at.%)	(1 1 1) peak position	Hardness (GPa)
0	100	36.86	13.95
8.4	91.5	36.72	16.08
12.6	87.4	36.59	25.64
17.9	82.1	36.58	18.22
25.3	74.7	36.56	20.31
36.8	63.2	36.49	23.61
47.0	53.0	–	12.33

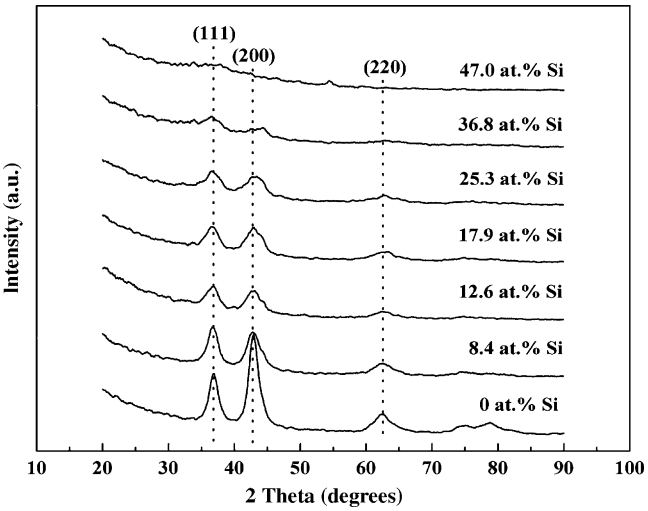

Fig. 1. X-ray diffraction patterns of the CrSiN films with various Si contents.

of the CrN film and can be well indexed using the cubic NaCl-type structure. It is interesting to note that there are no diffraction peaks corresponding to silicon-containing compounds (e.g. $CrSi_2$, Si and Si_3N_4), which indicates that the Si_3N_4 may exist in the form of amorphous. As the Si content in the CrSiN films increased, the diffraction peak intensities of CrN phase gradually reduced. The CrN (1 1 1) diffraction peaks shifted to lower angles as the Si contents increased up to 36.8 at.% Si/(Cr + Si) (Table 1). This could be due to that the added Si atoms were dissolved into CrN lattice [7]. Although the solubility limit of Si in the CrN phase was supposed to be very small, a certain amount of Si atoms could be dissolved into CrN crystal because the physical vapor deposition process was under non-equilibrium status. This might also increase the intrinsic stress of the films. The CrN (1 1 1) diffraction peaks shifted to lower angles as the Si contents increased up to 36.8 at.% Si/(Cr + Si) (Table 1). This could be due to that the added Si atoms were dissolved into CrN lattice [7]. Although the solubility limit of Si in the CrN phase was supposed to be very small, a certain amount of Si atoms could be dissolved into CrN crystal because the physical vapor deposition process was under non-equilibrium status. This might also increase the intrinsic stress of the films. In addition, the peak broadening phenomenon was also observed with the increase of Si content in CrN coatings. Such XRD peak broadening was believed to originate from the diminution of the grain size and/or the residual stress induced in the crystal lattice. The decrease of the crystallite size with increasing silicon content was attributed to the formation of stable nanostructure, composed of CrN crystal and amorphous Si_3N_4 matrix [6,10]. For the CrSiN film of 47.0 at.% Si, the XRD peaks disappear because the CrN crystals become too tiny to detect or the whole film become amorphous (Fig. 1). It seems that the existence of large content amorphous Si_3N_4 suppresses the formation of crystalline CrN, and thus the peaks of CrN crystals disappear.

The presence of the Si_3N_4 phase has been confirmed by infrared spectroscopy. Fig. 2 shows the FTIR spectra of CrSiN films with various Si contents. The CrN film without Si has a broad absorption band located at 400–600 cm^{-1} only, which is due to the vibration mode of the Cr–N bond [22]. In contrast, the FTIR spectra of the CrSiN films show not only a broad absorption band located at 400–600 cm^{-1}, but also a broad absorption band at 700–1100 cm^{-1}, which can be identified by different stretching vibration modes of the Si–N bonds. The deconvolution of the absorption band, given three Gaussian peaks centered at 800, 840 and 970 cm^{-1} (Fig. 3), was attributed to various vibrational modes of a-Si_3N_4 [23]. The

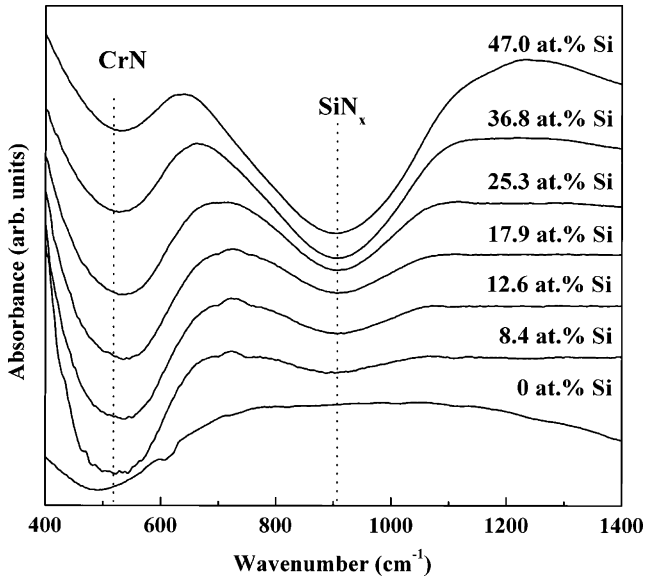

Fig. 2. FTIR absorbance spectra of the CrSiN films with various Si contents.

intensity of the Si–N bonds absorption peaks become much stronger compared to the intensity of the Cr–N bonds absorption peaks with the increase of the Si content in the films. These results further approved that the formation of large content a-Si_3N_4 matrix in the films with the increase of Si content.

In order to further clarify bonding status of the amorphous phase in CrSiN films, XPS analyses were performed. The C 1s peak of adventitious hydrogen carbon (binding energy = 284.8 eV) was taken as the reference in calibration of the binding energy. Fig. 4a shows the Si 2p XPS spectra of the CrSiN film with various Si contents. The peak corresponding to 101.8 eV, which was in good agreement with that of the Si_3N_4 compound [7], was observed. The peak intensities increased with the increase of Si content. No other peaks corresponding to Si–Si bond (99.28 eV) or Cr–Si bond (99.56 eV) were observed. However, the Si_3N_4 peaks were not found from XRD analysis as showed in Fig. 1. It indicated that amorphous Si_3N_4 existed in the films. This is in good agreement with the reported results in Refs. [6,7,15] where Si_3N_4 compounds

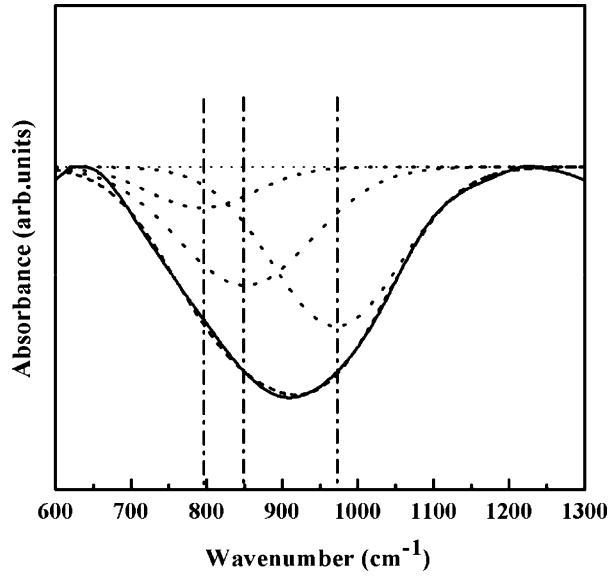

Fig. 3. The deconvolution of the Si–N absorption band for the CrSiN films with 47.0 at.% Si content.

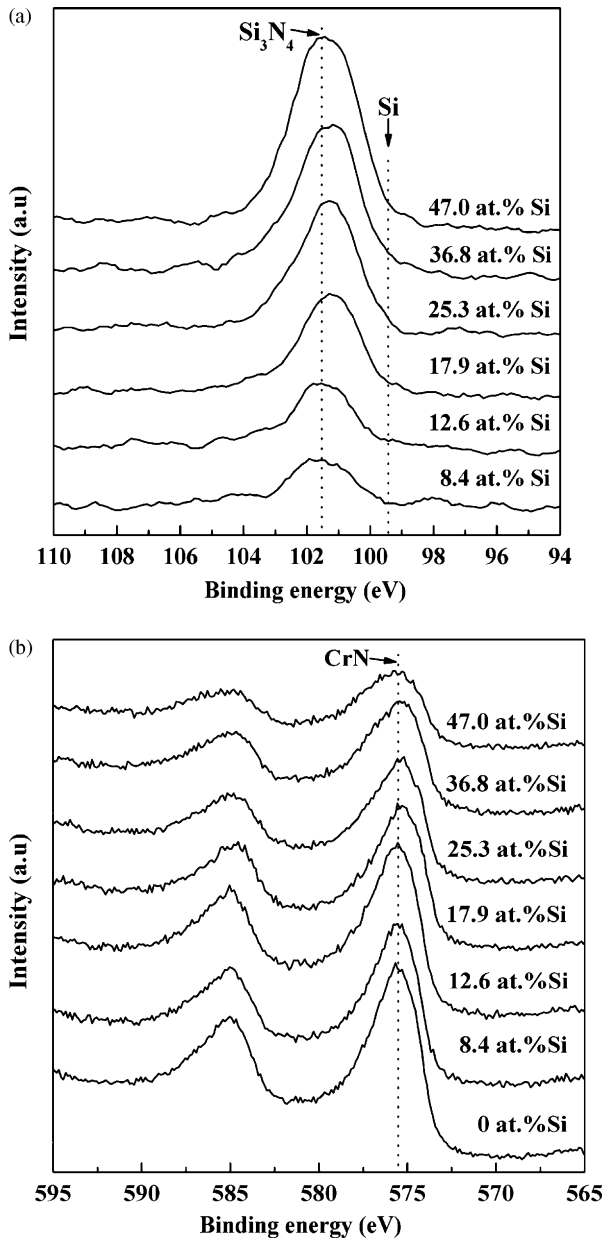

Fig. 4. XPS Si 2p and Cr 2p spectra of the CrSiN films with various Si contents.

are in the form of amorphous in CrSiN or TiSiN films. On the other hand, the peak corresponding to 575.8 eV was found to be that of stoichiometric CrN [24], and this peak intensities decreased with the increase of Si contents (Fig. 4b). It is reasonable to propose that the CrSiN films have a nanocomposite structure consisting of nanocrystalline CrN in amorphous Si_3N_4 matrix.

In order to investigate the influence of the doping Si on the microstructure of the CrSiN films, the cross-sectional profiles of the films were observed by FESEM. The cross-sectional micrographs of CrSiN films are shown in Fig. 5. The CrN film exhibited a continuous columnar structure, which consisted of columnar grains parallel to the growth direction in the order of about 100 nm (Fig. 5a). The CrSiN film with low Si/(Cr + Si) ratio (8.4%) (Fig. 5b) also exhibited columnar structure. However, it is clear that column propagation was interrupted by the further increase of Si and the granular structure can be observed in the CrSiN (Si/(Cr + Si) ratio of 25.3%) film (Fig. 5c). As the Si/(Cr + Si) ratio increased to 47.0%, neither columnar structure nor granular structure could be seen, and the coating exhibited an glassy-like appearance morphology.

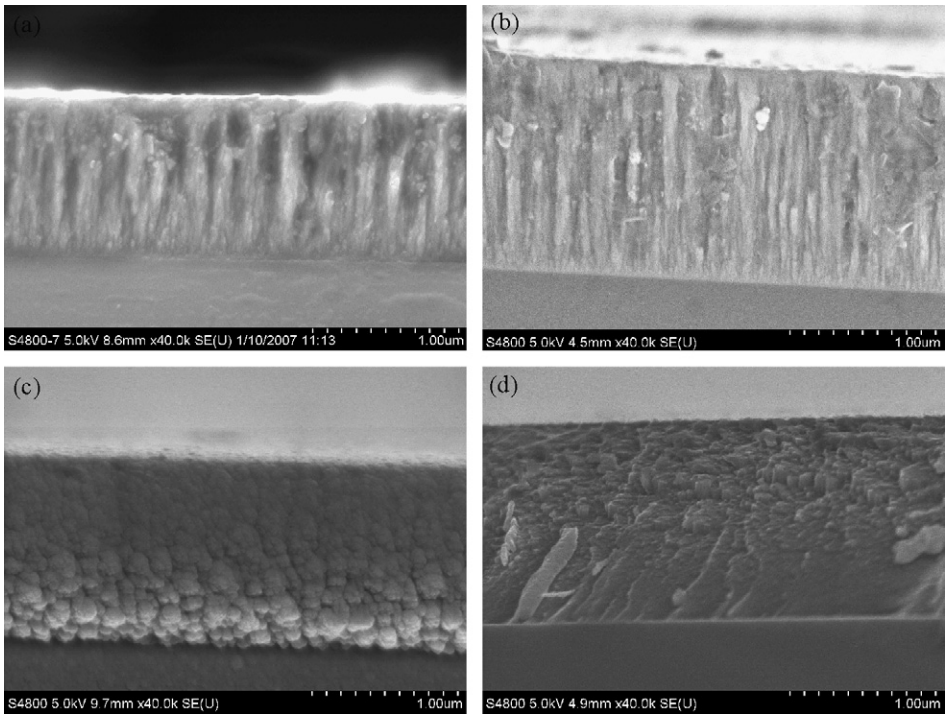

Fig. 5. SEM images of CrSiN films with (a) Si/(Cr + Si) ratio of 0%; (b) Si/(Cr + Si) ratio of 8.4%; (c) Si/(Cr + Si) ratio of 25.3%; (d) Si/(Cr + Si) ratio of 47.0%.

3.2. Mechanical evaluation of CrSiN films

The hardness of the CrSiN films was measured by nanoindentation test. The hardness of the CrN film produced using this deposition conditions described in this paper was about 13 GPa. Fig. 6 shows the curves for the hardness and Young's modulus against Si/(Cr + Si) ratio of CrSiN films. As the Si content increased, the hardness of the CrSiN films increased from ~13 GPa for CrN to the first peak with the maximum value of approximately 25 GPa at the Si/(Cr + Si) ratio of 12.6%, and then decreased until 18 at.% [Si/(Cr + Si)], which was attributed to the increase of the fraction of amorphous SiNx phase into the coating. However, with the further increase of the Si content, the hardness increased again and second peak appeared at Si/(Cr + Si) ratio of 36.8%. The modulus values of the CrSiN films with the increase of the Si content also showed a similar profile with the hardness. The two hardness peaks suggest that different hardness mechanisms might be involved. The first hardness peak of CrSiN films with the Si/(Cr + Si) ratio about 10% must be related with the refinement of CrN crystallines. According to the generic design concept [6,10], this high hardness is based on the combination of the absence of dislocation activity in the small CrN nanocrystals and blocking of grain boundary sliding by the formation of a strong interface between the two phases. In addition, as seen in Table 1, The CrN (1 1 1) diffraction peaks shifted to lower angles monotonously with the increase of Si content. This illustrated that the films possessed relatively high stresses and the stress increased monotonously with the Si content [25]. The film with relative high stress may also attribute the high hardness. The 2nd peak may involve the existence of Si phase and amorphous CrN phase. At higher silicon content (Si/(Cr + Si) ratio of 47.0%), the amorphous films usually have disordered network with low density and could not sustain high loading during indentation, and thus the hardness was low. The hardness of the CrSiN films lower than the theoretical value resulted from impurities such as oxygen and carbon. Also the defects and voids, cracks around/or contain the crystal determined from this non-equilibrium PVD method, could propagate along the weak boundaries under indentation force, thus high hardness as the bulk material could not be obtained in the thin films.

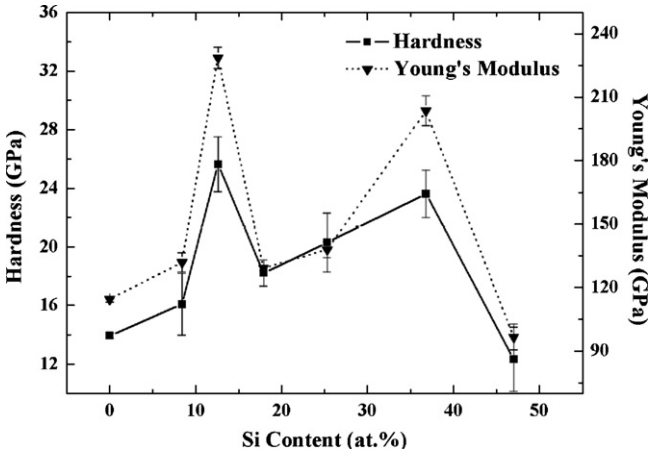

Fig. 6. Hardness of CrSiN films as a function of Si contents.

4. Conclusions

CrSiN films with various Si contents were deposited by medium frequency reactive magnetron sputtering. The CrN crystalline size decreases and its crystal structure changes from crystalline to amorphous phase as the Si content increases. No XRD peaks corresponding to Si_3N_4 or other silicide compounds were observed. The FTIR and XPS results suggest that Si_3N_4 phase exists as an amorphous phase in the films. Cross-sectional images showed that the film growed up from continuous columnar structure, granular structure to glassy-like appearance morphology with the increase of silicon content. The two hardness peaks of the films were attributed to the nanocomposite and the relatively high stress.

Acknowledgments

The authors are grateful to the National Natural Science Foundation of China (No. 50772115 and No. 50823008) for financial support of this research work.

References

[1] C. Rebholz, H. Ziegele, A. Leyland, A. Matthew, Surf. Coat. Technol. 115 (1999) 222.
[2] G.A. Zhang, P.X. Yan, P. Wang, Y.M. Chen, J.Y. Zhang, Mater. Sci. Eng. A 460–461 (2007) 301.
[3] Y.J. Zhang, P.X. Yan, Z.G. Wu, J.W. Xu, W.W. Zhang, X. Li, W.M. Liu, Q.J. Xue, J. Vac. Sci. Technol. A 22 (6) (2004) 2419–2423.
[4] H.C. Barshilia, A. Jain, K.S. Rajam, Vacuum 72 (2004) 241–248.
[5] G.A. Zhang, Z.G. Wu, M.X. Wang, X.Y. Fan, J. Wang, P.X. Yan, Appl. Surf. Sci. 253 (2007) 8835–8840.
[6] S. Veprek, S. Reiprich, Thin Solid Films 268 (1995) 64.
[7] J.H. Park, W.S. Chung, Y.-R. Cho, K.H. Kim, Surf. Coat. Technol. 188–189 (2004) 425.
[8] G.-S. Kim, B.-S. Kim, S.-Y. Lee, Surf. Coat. Technol. 200 (2005) 1814–1818.
[9] M. Diserens, J. Patscheider, F. Lévy, Surf. Coat. Technol. 108–109 (1998) 241.
[10] S. Veprek, J. Vac. Sci. Technol. A 17 (1999) 2401.
[11] E. Martinez, R. Sanjines, A. Karimi, J. Esteve, F. Levy, Surf. Coat. Technol. 180–181 (2004) 570–574.
[12] D. Pilloud, J.F. Pierson, J. Takadoum, Thin Solid Films 496 (2006) 445–449.
[13] Y.S. Dong, Y. Liu, J.W. Dai, G.Y. Li, Appl. Surf. Sci. 252 (2006) 5215–5219.
[14] Q. Liu, Q.F. Fang, F.J. Liang, J.X. Wang, J.F. Yang, C. Li, Surf. Coat. Technol. 201 (2006) 1894–1898.
[15] H.Y. Lee, W.S. Jung, J.G. Han, S.M. Seo, J.H. Kim, Y.H. Bae, Surf. Coat. Technol. 200 (2005 1026).
[16] J.W. Kim, K.H. Kim, D.B. Lee, J.J. Moore, Surf. Coat. Technol. 200 (2006) 6702.
[17] K. Yamamoto, T. Sato, M. Takeda, Surf. Coat. Technol. 193 (2005) 167.
[18] D. Mercs, N. Bonasso, S. Naamane, J.-M. Bordes, C. Coddet, Surf. Coat. Technol. 200 (2005) 403.
[19] S.Y. Lee, B.S. Kim, S.D. Kim, G.S. Kim, Y.S. Hong, Thin Solid Films 506–507 (2006) 192.
[20] P. Wang, X. Wang, T. Xu, W. Liu, J. Zhang, Thin Solid Films 515 (2007) 6899.
[21] W.C. Oliver, G.M. Pharr, J. Mater. Res. 7 (1992) 1564.
[22] O. Banakh, P.E. Schmid, R. Sanjines, F. Levy, Surf. Coat. Technol. 163–164 (2003) 57.
[23] Y.C. Liu, K. Furukawa, D.W. Gao, H. Nakashima, K. Uchino, K. Muraoka, Appl. Surf. Sci. 121–122 (1997) 233.
[24] Q.G. Zhou, X.D. Bai, X.W. Chen, D.Q. Peng, Y.H. Ling, D.R. Wang, Appl. Surf. Sci. 211 (2003) 293.
[25] D. Mercs, P. Briois, V. Demange, S. Lamy, C. Coddet, Surf. Coat. Technol. 201 (2007) 6970.